STM-excited electroluminescence and spectroscopy on organic materials for display applications

by S. F. Alvarado L. Rossi P. Müller P. F. Seidler W. Riess

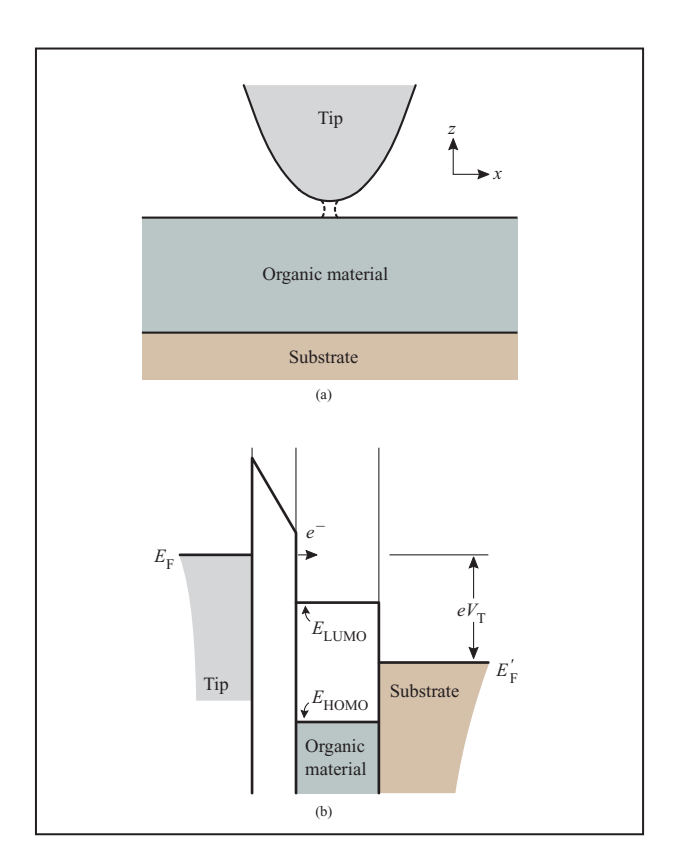
We present an overview of the current status of our work on scanning-tunnelingmicroscope-based (STM) spectroscopy and electroluminescence (EL) excitation to study the physical and electronic structure of organic materials used in organic lightemitting devices (OLEDs). By these means we probe the critical device parameters in chargecarrier injection and transport, i.e., the height of the barrier for charge-carrier injection at interfaces between different materials and the energy gap between positive and negative polaronic states. In combination with optical absorption measurements, we gauge the exciton binding energy, a parameter that determines energy transport and EL efficiency. In STM experiments involving organic EL excitation, the tip functions as an OLED electrode in a highly localized fashion, allowing one to map the spatial distribution of the EL intensity across thin-film samples with nanometer lateral resolution as well as to measure the local EL emission spectra and the influence of thin-film morphology.

1. Introduction

Since the recent development of high-efficiency organic light-emitting devices (OLEDs), many experimental and theoretical investigations have been undertaken to elucidate the underlying fundamental physical processes. Knowledge of the relative alignment of the energy levels at interfaces between organic materials is crucial in order to understand the device operation and, in particular, the physics of charge-carrier injection, transport, and radiative recombination, with the ultimate goal of improving electroluminescence efficiency. The alignment of the highest occupied molecular orbitals (HOMOs) at the interfaces of an OLED is usually estimated from the ionization potential (IP) of each material by using the Schottky-Mott rule [1], which assumes that the energy levels correspond to a common vacuum level (CVL), thus neglecting surface, interface, and charge-transfer effects. These effects induce a significant shift of the energy levels with respect to the CVL predictions. The alignment of the lowest unoccupied molecular orbital (LUMO) is determined by adding the bandgap, measured from optical absorption, to the HOMO energy, a procedure that neglects the exciton binding energy as well as molecular levels of optically forbidden electronic transitions. This

©Copyright 2001 by International Business Machines Corporation. Copying in printed form for private use is permitted without payment of royalty provided that (1) each reproduction is done without alteration and (2) the *Journal* reference and IBM copyright notice are included on the first page. The title and abstract, but no other portions, of this paper may be copied or distributed royalty free without further permission by computer-based and other information-service systems. Permission to *republish* any other portion of this paper must be obtained from the Editor.

0018-8646/01/\$5.00 © 2001 IBM



Fiaure 1

(a) Geometry and (b) energy diagram for a typical STM configuration, in which charge injection into the organic material occurs via tunneling through a vacuum barrier. $V_{\rm T}$ is the applied tunnel bias relative to the Fermi level $(E_{\rm F}')$ of the substrate. In the case of negative tip polarity shown here, electrons are injected from the Fermi level of the tip $(E_{\rm F})$ into the empty levels of the organic material. $E_{\rm LUMO}$ $(E_{\rm HOMO})$ is the energy of the lowest (highest) molecular orbital of the organic material.

method for modeling OLED energy diagrams is a useful first approximation, but can lead to significant errors. For instance, studies performed using techniques such as ultraviolet photoemission spectroscopy (UPS) [2-7], internal photoemission [8, 9], and scanning tunneling microscope (STM) spectroscopy [10-12] show clear evidence of significant deviations from the CVL rule for organic-metal and organic-organic interfaces. In addition, experimental studies show that the actual gap for chargecarrier injection into organic materials can be significantly larger than the optical bandgap [8, 12]. The excess energy is due to the binding energy of the singlet exciton, $E_{\rm h}$. For example, for the commonly used material poly(p-phenylenevinylene) (PPV) and its derivatives, $E_{\rm b}$ has been determined by a number of different techniques, and values between 200 and 500 meV have been obtained [8, 12–16]. Other measurements, however, suggest values

as low as 25 meV [17] or as high as 1 eV [18, 19]. These experimental results do not address the question of what the physical and chemical phenomena are that determine the energy-level alignment and transport properties for organic–organic and organic–metal interfaces.

In this paper we show how STM-based techniques can be employed to probe the electronic and transport properties of organic materials, which can lead to new attempts to answer this question. In fact, one important capability of the new STM-based techniques described here is that they allow one to take direct measurements of the molecular-level alignment of the filled and empty states of all of the interfaces of a multilayer OLED. A technique that allows the alignment of the empty states to be determined in a direct way is particularly welcome, because photoemission spectroscopy techniques have so far proved useful only as probes of the occupied levels of organic materials. Here we discuss results obtained with thin films of organic materials used in the prototypical Kodak OLED structure consisting of a vapordeposited stack of copper phthalocyanine (CuPc), N,N'-di(naphthalen-1-yl)-N,N'-diphenyl-benzidine (NPB), and tris(8-hydroxyquinolato) aluminum (Alq₃) thin-film layers [20]. Each of the organic layers in the OLED fulfills a specific function. The electroluminescent layer is Alq₃, a highly efficient fluorescent material that predominantly transports electrons, whereas NPB is a good holeconducting material. CuPc is a buffer layer inserted between the anode and the NPB layer to improve device stability [20, 21]. Crucial for the performance of the device is the relative alignment of the energy levels of each of its components. Of particular interest is the Alq₃-NPB interface, where the energy levels form a potential barrier that confines electrons on the Alq, side and holes on the NPB side; i.e., an accumulation region is formed that promotes radiative recombination [22].

2. Charge-carrier injection from the STM tip into organic materials

A basic condition in scanning tunneling microscopy and spectroscopy is that the tunneling resistance $R_{\rm T} = V_{\rm T}/i_{\rm T}$ has to be much higher than the resistive losses associated with current flow through the sample (spreading resistance). The charge-injection process takes place by means of tunneling through a vacuum potential barrier (Figure 1). As the applied bias voltage, $V_{\rm T}$, drops fully at the tunneling barrier, the charge-carrier injection energy can be tuned through the polarity and magnitude of $V_{\rm T}$. This is the model underlying the spectroscopy technique for the determination of the density of states in the surface region by means of i-V curves collected with the STM-feedback loop disconnected [23]. If the resistive losses within the organic material are allowed to become comparable to $R_{\rm T}$, however, the surfaces of the tip and the

sample can come into close proximity and make physical contact, causing the vacuum barrier to collapse. In the following we discuss charge-carrier injection as well as the electric-field distribution for this particular case. In the subsequent sections we discuss how this injection mode can be used to locally probe the transport properties of soft organic materials as well as electronic excitations and molecular energy levels at organic interfaces.

We begin by noting that when the tip makes contact with the organic surface, its Fermi level is pinned, typically at an energy within the energy gap. This gives rise to the formation of a Schottky barrier, and the bias voltage drops fully within the organic material. Figure 2 shows geometry and energy diagrams for the case of negative tip polarity (tip negative, $V_{\rm\scriptscriptstyle T} < 0$, relative to the Fermi level of the anode) and a magnitude of $V_{\rm T}$ such that the Fermi level of the tip is above the threshold for injection into the lowest electron polaron state of the organic material. Here the average field at the injection spot is $E_{\rm m} = (V_{\rm T} - V_{\rm bi})/d$, where $V_{\rm bi}$ is the tip-substrate contact potential and d the distance between the tip apex and the substrate when the tip is in contact with the organic material. The energy diagram corresponds to that of a single-layer OLED, but with one significant difference: The strength of the electric field is much higher at the apex of a tip than at a planar electrode interface. In this configuration, charge carriers are injected by tunneling through the Schottky barrier into polaron states of the organic material [24]. Charge injection from Schottky barriers into organic material has been the topic of several theoretical studies; see for instance References [24] and [25].

In the spherical apex approximation, the electric field near a tip apex of effective radius R drops off as $1/(R+r)^n$, with distance r from the tip, where n=2 for the case of ohmic and n=1/2 for space-charge-limited current flow [26]. This field distribution, characterized by an enhanced electric field at the tip apex, the radius of which is typically a few to several tens of nanometers, is the reason why it is possible to inject extremely high current densities in STM experiments. These current densities are estimated to be in the range of j=10– 10^4 A/cm², orders of magnitude higher than those used in standard planar-contact OLED devices, where typically j<1 A/cm². The ratio between the field at the apex and the field at the substrate, E_T and E_S , is approximately

$$E_{\mathrm{T}}/E_{\mathrm{S}} \cong [(\kappa R + d)/\kappa R]^{n},$$

where κ is a modifying factor to account for the geometry of the real system. For instance, $\kappa > 1$ for $R \ll d$ due to the effect of the tip's shaft, whereas $\kappa < 1$ for $R \cong d$ due to the proximity of the planar substrate. Note that the

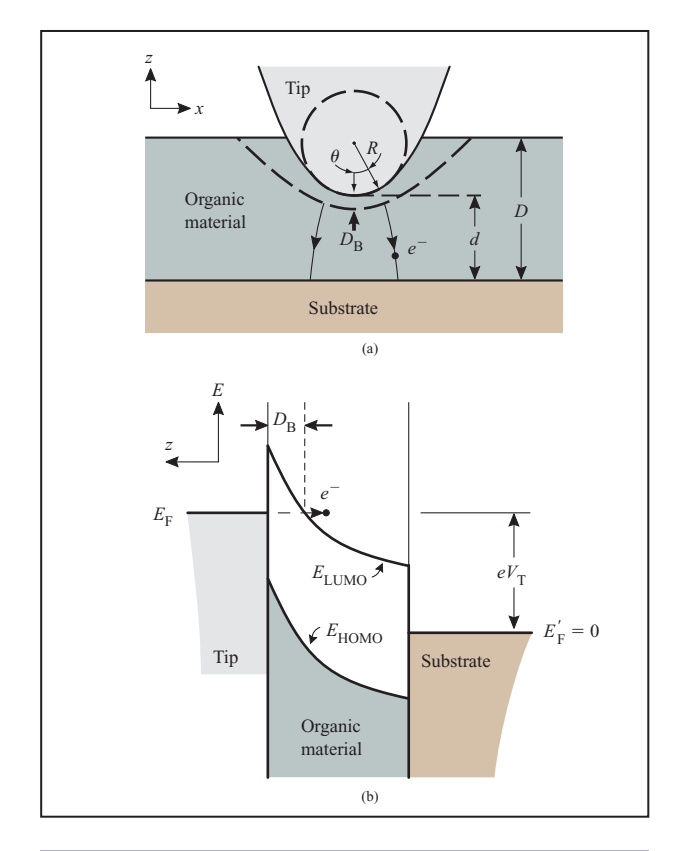


Figure 2

(a) Geometry and (b) energy diagram for tunneling in the point contact case. Injection of charge carriers into a thin film of thickness D of organic material occurs via tunneling through a Schottky barrier of thickness $D_{\rm B}$ (image force contributions to the potential not shown). Predominant injection from the tip of apex radius R takes place within a half angle θ . The distance between the tip apex and the substrate is d < D.

actual injection process can be either thermionic emission or tunneling [27], depending on the barrier heights, field strengths at the injection interface (which depend on the actual sharpness of the tip), and temperature. For barrier heights of approximately 1 eV and average fields in the neighborhood of 0.1–1 V/nm, typical values in the experiments described below, we expect predominantly tunneling injection [27], whereas thermionic emission might become significant for barrier heights well below 1 eV.

The question arises as to what is the current balance for the point-contact injection geometry compared to the planar OLED case. The electric field is significantly higher at the tip apex than at the substrate interface, which translates exponentially into a much higher injection probability of charge carriers across the Schottky barrier from the tip than from the substrate. Consequently, the current passing through the tip/organic material/substrate system is expected to be predominantly monopolar. There

¹ S. F. Alvarado, work in preparation.

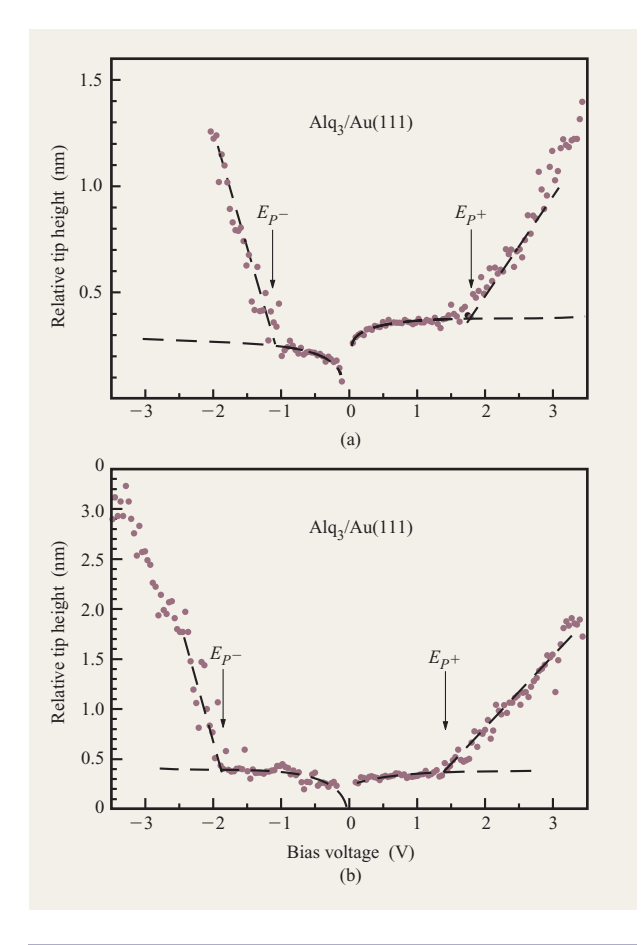


Figure 3

z-V curves collected on an Alq₃ thin film deposited on an Au(111) substrate. The dashed curve represents the typical tip displacement measured for the clean Au(111) substrate. The curves in panels (a) and (b) were collected at different locations of the sample. The threshold for injection of charge carriers into electron (E_p-) and hole polaron (E_p+) states is marked by a sharp decrease of the slope of the z-V curve. The shift in charge injection thresholds is discussed in the text.

are, however, some requirements for this condition to exist; for example, R should be small, and the barrier height for oppositely charged carrier injection from the substrate should not be much smaller than the barrier height at the tip. 1

Regarding tip penetration, it is clear that if the magnitude of $V_{\rm T}$ is decreased while keeping $i_{\rm T}$ constant, the feedback loop causes the tip to move into the sample, decreasing d to counterbalance the decrease in $R_{\rm T}$. Here the requirement is that the tip motion should compensate for the electric field reduction associated with the change in $V_{\rm T}$ to maintain constant tunneling current flow across the barrier. Note that as the tip contact area increases

with decreasing d, the electric field required for injection and transport is somewhat lowered as the tip moves into the sample. This electric field reduction is relatively small, however, because of the exponential dependence of the injection probability on the electric field. In addition, since the electric field is strongest at the tip apex and decreases with injection angle θ , the thickness $(D_{\rm B})$ is lowest for tunneling in the $\theta=0$ direction. This implies that the effective injection area does not change strongly with d, except in the initial stages of contact, $d\cong D$, where D is the thickness of the thin film (see Figure 2).

3. Measurement of the barrier height for charge-carrier injection

The measurement of z–V curves can be used as a spectroscopy technique to probe the density of states of the material in a manner that differs from the standard i-V spectroscopy technique. More specifically, as the magnitude of the bias voltage is decreased, the tip penetrates the organic material and can inject charge carriers in the neighborhood of the substrate interface [Figure 2(b)]. Charge-carrier injection into the organic material is possible until, at a characteristic threshold voltage at which the Fermi level of the tip moves into the forbidden energy gap at the interface with the substrate, the tip penetrates deeply into the organic material, reaching the interface region in which charge carriers can be injected into the substrate either by directly tunneling into it or via nonresonant tunneling through molecules in contact with it. This threshold voltage $(V_{\rm th})$, typically identified by a sharp decrease in the slope (dz/dV) of the z-V curve, marks the threshold for injection into the lowest electron polaron state for negative tip polarity, and is thus a measure of the potential barrier for electron injection at the buried interface of the organic material [Figure 2(b)]. Repeating this gedanken experiment for positive tip polarity, we can convince ourselves that the barrier for hole injection into polaronic states can be measured using the same procedure. We emphasize that the z–V technique works only for soft materials that yield to the pressure exerted by the tip [28].

Figure 3 shows z-V spectra collected on $\mathrm{Alq_3}$ thin films deposited on a Au thin film on a mica substrate. The Au thin film had previously been annealed at $350^{\circ}\mathrm{C}$ to produce atomically flat $\mathrm{Au}(111)$ facets a few hundred nm in lateral dimension. The typical z-V tip displacement for a clean $\mathrm{Au}(111)$ facet is shown as a dashed curve. The measurements on $\mathrm{Alq_3}$ thin films yield a threshold energy of $E_{p^-}=1.15\pm0.180$ eV for electron injection, and $E_{p^+}=-1.81\pm0.25$ eV for hole injection, relative to the Fermi level of the $\mathrm{Au}(111)$ substrate. From these results we can directly determine the bandgap for injection of charge carriers into polaron states, the so-called single-particle energy gap [8]. Note that this is the energy gap

¹S. F. Alvarado, work in preparation.

that one should use to model the energy diagram of OLEDs. Figures 4(a) and 4(b) show histograms of the electron injection threshold of Alq, thin films deposited on Au(111) and Ag(111) substrates. Each event represents a threshold measurement taken on a different spot of the sample. The distribution reveals the existence of regions where the injection threshold for electrons is 0.6 to 0.7 eV higher. In these regions the energy gap appears to be approximately 80 meV larger (on average). A possible cause for this shift is the occurrence of various Alq, morphologies [29] or shape isomer domains, which can have different interactions with the substrate. In Section 6 we discuss STM-excited electroluminescence spectroscopy measurements that provide further evidence for this interpretation. We note that owing for instance to contaminants, local variations of the substrate properties can also induce a shift of the energy levels of the molecular orbitals. However, as the measurements were performed at ultrahigh-vacuum conditions on samples grown in situ, the latter explanation seems implausible.

In the following we compare the values of the barrier heights determined by z-V spectroscopy with the predictions of the CVL approximation, bearing in mind that, given the uncertainties of our measurements and those of others, only differences of more than 0.3-0.4 eV are significant. The scatter of the IP values for organic materials reported by different groups is of this magnitude. Despite these relatively important shifts of the injection threshold, we find that the energy levels of Alq, clearly align below the CVL estimate for the Au(111) substrate. The barrier height for electron injection of 2-2.5 eV is estimated from the IPs of 5.31 eV for Au(111) [30], 5.57-6.0 eV for Alq, [2, 3, 31-35], and the singleparticle bandgap of 2.96 ± 0.13 eV (see below). In addition, we see that the electron injection barrier is approximately 200 meV higher on Au(111) than on Ag(111). The magnitude of the shift, however, is smaller than the value of approximately 600 meV calculated by taking the difference between the work functions of the Ag(111) (4.74 eV [30]) and Au(111) surfaces. These deviations from the simple CVL model indicate the effect of image forces or the formation of a dipole layer at the surface, due to negative charge transfer from Alq, to the metal substrate. A similar result for hole injection also shows the invalidity of the CVL model, and our values for the threshold of the occupied states (see above) confirm the results of UPS measurements on the Alq₃/Au(111) system [2-4].

4. Probing the exciton binding energy

The combination of a hole polaron and an electron polaron (P^+, P^-) , respectively) results in the formation of an exciton. The exciton binding energy has been defined [36] as $E_{\rm b} = E_{\rm esp} - E_{\rm a}$, where $E_{\rm esp}$, the difference between

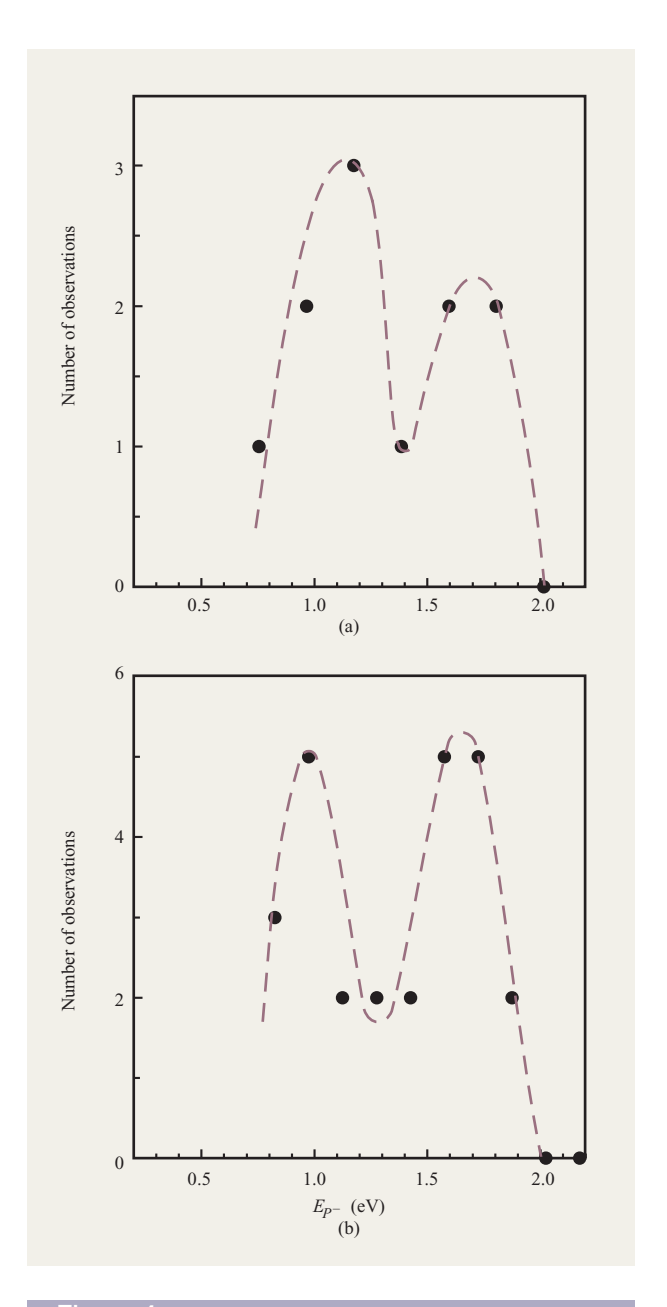


Figure 4

Histograms of the injection threshold of electrons into an Alq_3 thin film deposited on (a) Au(111) and (b) Ag(111) substrate. The dashed lines are guides to the eye.

the electron and hole polaron energies, is called the single-particle energy gap [8], and $E_{\rm a}$ is the energy required to create a molecular exciton as determined from optical absorption spectra (the diagram in **Figure 5** illustrates this definition). Here HOMO and LUMO represent the one-electron band picture, which neglects Coulomb and exchange interactions as well as molecular relaxation effects. Supplying the exciton with energy $E_{\rm b}$

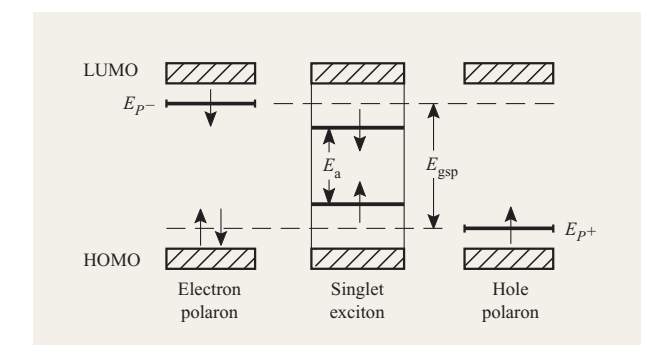


Figure 5

Diagram illustrating the definition used to determine the exciton binding energy $E_{\rm b}$. The parameter $E_{\rm gsp}$ is the single-particle bandgap determined from z-V curves (Figure 3); $E_{\rm a}$ is the optical absorption threshold. Adapted from [12(a)].

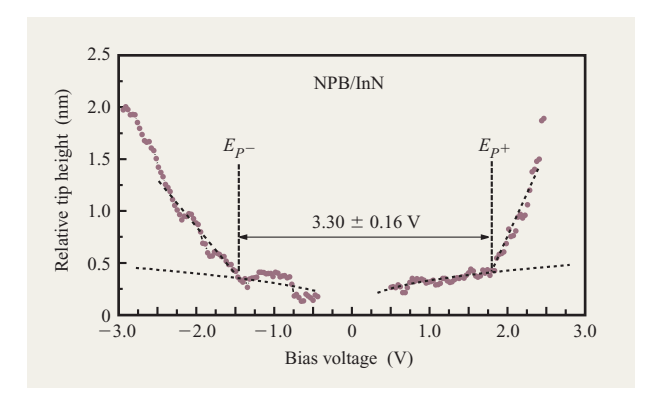


Figure 6

z–V curves collected on an NPB thin film deposited on an InN substrate.

creates a pair of oppositely charged polarons. In an organic material the radiative decay of a singlet exciton results in the emission of a photon. From a series of z–V measurements as well as from electroluminescence intensity vs. $V_{\rm T}$ measurements (described below), we find that $E_{\rm gsp}=2.96\pm0.13$ eV for Alq $_{\rm 3}$. Combining this result with the threshold for optical absorption of Alq $_{\rm 3}$, $E_{\rm a}\cong2.75$ eV, we obtain $E_{\rm b}=220\pm130$ meV. This result compares well with the theoretical results of ab initio calculations by Curioni and Andreoni. Note that the polaron self-trapping energy is expected to be different for the facial and the meridianal isomers [37].

Figure 6 shows z–V measurements performed on a thin film of NPB deposited on an InN substrate. For this

material we find $E_{\rm gsp}=3.30\pm0.16$ eV. The optical absorption gap of this material is $E_{\rm a}=3.0$ eV [38, 39], from which we obtain $E_{\rm b}=300\pm160$ meV. The results for CuPc single layers [40] indicate that the gap for charge-carrier injection is *smaller* than the optical gap, $E_{\rm a}=1.6$ –1.7 eV (see next section) [41]. This fact is evidence that the injection and transport involve molecular orbital states not accessible by optical means [40].

5. STM as a probe of local conductivity

The rate of penetration, dz/dV, deserves some attention because it depends on local charge-carrier transport characteristics of the material, as shown in the following. We begin by considering the voltage bias V_c at which the tunneling barrier collapses, noting that this point is marked by an increase of the slope of z–V because of the onset of penetration. For a given constant $i_{\scriptscriptstyle T}$ and hypothetical thin films of equal thickness D, it is easy to see that in order to sustain the current flow through the injection region, a lower electric field is required for highconductance than for low-conductance materials. In other words, $D/|V_{\rm ch}-V_{\rm th}|>D/|V_{\rm cl}-V_{\rm th}|$, where $V_{\rm ch}$ and $V_{\rm cl}$ denote the voltages at which the tunneling barrier collapses for high- and low-conductance materials, respectively. Thus, in contact mode we expect the average slope of the z–V curves to be directly proportional to the conductivity of the sample. This implies that in pointcontact mode, the z–V curves can yield information about the transport properties of organic materials. From the above considerations we can additionally conclude that for a given sample conductance, the rate of penetration is proportional to the tunnel resistance, i.e., inversely proportional to i_{T} , a fact that we have verified experimentally [40].

In the following we compare z–V measurements performed on organic materials with very different transport properties, namely the hole conductors CuPc and NPB and the electron conductor Alq3. We also show how relative electron and hole mobilities can be probed by means of this technique. Figure 7(a) displays a typical z-V curve collected on a CuPc thin film deposited on a Au(111) substrate. Figure 7(b) depicts the surface crystal structure of one of the polymorphic CuPc crystallites on which the curve was collected [40]. For these measurements the bias voltage was ramped with decreasing magnitude for each polarity. Each z-V run begins with the tip biased at a potential difference high enough to ensure that the tip is above the surface of the organic film to avoid modifying or damaging the organic thin-film structure before the actual collection of data. Typical z–V curves for a clean Au(111) substrate are shown as dashed lines. The height difference between the

² A. Curioni and W. Andreoni, work in preparation.

two curves in the high-voltage region is an approximate measure of the local thickness of the organic thin film. At high bias voltages, the molecules at the free surface of the thin film can be clearly imaged [Figure 7(b)]. As the bias voltage is decreased, we observe that the tip moves into the thin film in a step-like fashion, initially by only one or two molecular spacings. In some cases the z–Vcurves exhibit several step-like transitions prior to full penetration [Figure 7(a)]. A striking feature of the z–Vcurves is the steepness of the curves near threshold, $dz/dV \approx 2 \times 10^2$ nm/V. Actually, the z-V curves collected on CuPc resemble the ideal step function expected for a highly conducting material with a bandgap: In the high-voltage range, the tip approximately follows the shallow z–V displacement typical of a clean metallic surface until it suddenly penetrates the organic material when its Fermi level shifts to energies very close to the forbidden gap.

In comparison, z-V curves collected on Alq, or NPB thin films exhibit a much shallower slope, typically 1.4-3 nm/V; see Figure 3 and Figure 6. As discussed above, these results indicate that the conductivity of CuPc is much higher than that of Alq₃. This is indeed the case: The mobility of the majority charge carriers of CuPc, μ_h , is in the realm of 10^{-3} cm² V⁻¹ s⁻¹ (compare for example [42]), whereas that of Alq₃ [43, 44] is $\mu_a \le 10^{-4} \text{ cm}^2 \text{ V}^{-1} \text{ s}^{-1}$ at high electric fields. Note, additionally, that the slope of the z–V curve for Alq, is steeper for electron than for hole injection, indicating that the resistivity for electron transport is lower than for hole transport. This is in agreement with experimental results showing that the electron mobility is about two orders of magnitude higher than the hole mobility in this material (compare for example [44]). On the other hand, measurements on the hole conductor NPB, shown in Figure 6, show the reverse trend: The slope of the z–V curve is steeper for hole than for electron injection, as one would expect when the hole mobility is greater than the electron mobility.

The above experimental results show that the z-V curves can be used to characterize the transport properties of organic materials. For a more quantitative interpretation of the results, however, one has to take into account that the slope of the z-V curve can be influenced by various factors, for instance a) the actual height and thickness of the injection barrier, the latter of which is also sensitive to the sharpness of the tip; and b) the relatively strong field dependence of the charge-carrier mobility typical of amorphous organic materials with low mobility. Finally, we note that the actual value of the slope of the z-V curves is found to depend on the particular spot on which the curve is taken, showing that there are quantifiable in-plane variations of the transport properties of the thin film.

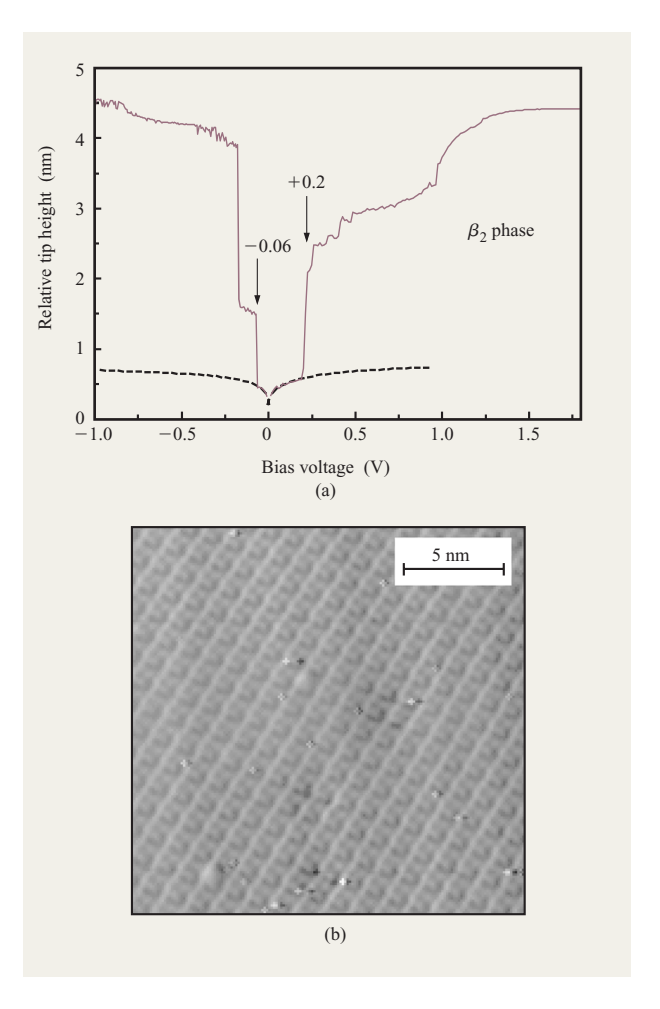


Figure 7

(a) z–V curves collected on a CuPc thin film deposited on an Au(111) substrate. The difference between the z–V curves of the CuPc sample (solid curve) and the clean substrate (dashed curve) at high bias voltages is an approximate measure of the thickness of the CuPc layer. (b) Typical in-plane crystal structure of the CuPc crystallites on which this measurement was made. Reprinted from [40], © 2001, with permission from Elsevier Science.

6. Electroluminescence generation by chargecarrier injection from the STM tip

The possibility of using an STM to generate electroluminescence (EL) with nanometer spatial resolution and thus to probe the electronic properties of organic materials has been demonstrated in experiments on various materials [10, 11, 45–48]. In STM-excited luminescence (STL) on organic materials, charge carriers from the tip tunnel into polaron states and, by combining with carriers of opposite polarity injected from the substrate, form excitons that can decay radiatively. Four kinds of STL experiments have been performed: 1) simultaneous collection of topography and wavelength-

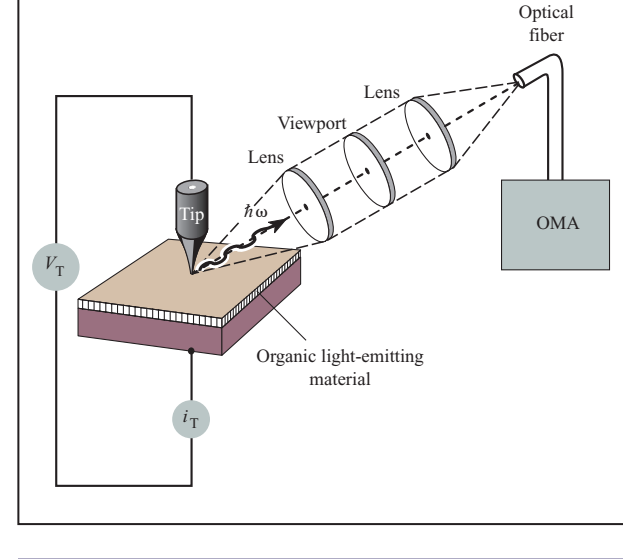


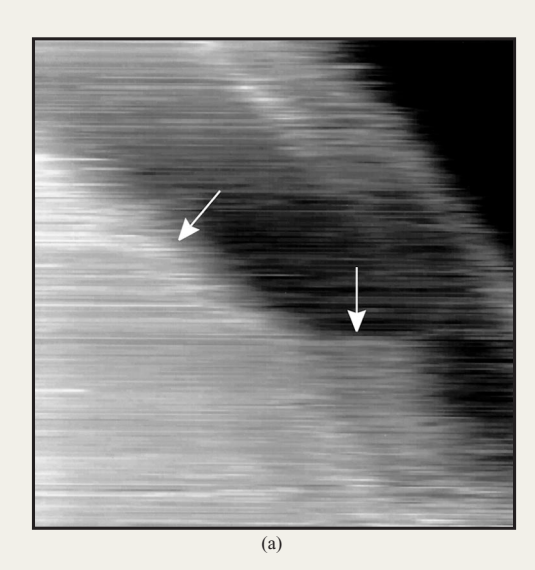
Figure 8

Schematics of the STM-excited electroluminescence setup. For wavelength-integrated intensity measurements, the optical fiber and optical multichannel analyzer (OMA) are replaced by an avalanche photodiode.

integrated EL intensity $(I_{\rm L})$ maps; 2) measurements of $I_{\rm L}$ vs. $V_{\rm T}$ curves; 3) EL spectroscopy, in which wavelength-resolved spectra are collected at different spots of the sample; and 4) EL intensity decay with time for charge-carrier injection at a fixed point of the sample. The experimental setup is shown schematically in **Figure 8** (for experimental details, see [11]).

We begin by briefly discussing the surface morphology of the Alq, thin films deposited on Au(111) substrates and its effect on the spectral distribution of the EL. The STM images reveal that the surfaces of thin films of Alq. exhibit different morphological features even on the same sample and within regions separated by less than 1 μ m. As an example, images collected on neighboring spots of a thin film approximately 5 nm thick are shown in Figure 9. The surface region shown in Figure 9(a) exhibits flat domains with a roughness of 0.11 nm (rms) where terraces can be identified. In some cases these domains exhibit parallelepiped-like features approximately 10 nm wide and 100 nm long. The heights of these features as well as those of the terraces appear to be defined by molecular layers of thicknesses in the range from 0.52 to 0.7 nm, indicating varying molecular packing [29]. On other regions of the samples, however, no terraces can be identified, and the surface corrugation is significantly higher [Figure 9(b)]. The formation of flat molecular domains and terraces seems to predominate in thinner films. For instance, for a film of thickness $D \cong 2.5$ nm, we

found regions of the organic layer so uniform and smooth that the atomically flat terraces of the underlying Au(111) substrate, in some cases even its herringbone surface reconstruction [49], are mimicked on their surface. Still, we found no clear evidence of in-plane crystalline order at the molecular level in our samples, which indicates that the thin films do not have a strong tendency to crystallize, but rather that they are probably disordered or amorphous in the plane of the terraces. Conversely, for films much thicker than 5 to 7 nm, where the absolute surface



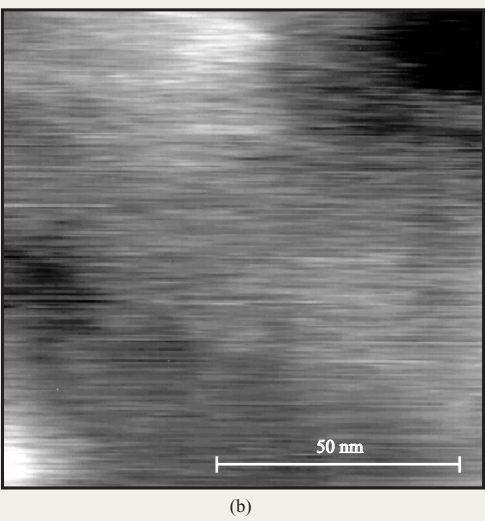


Figure 9

STM topographs of an Alq_3 -coated Au(111) surface showing (a) smooth terraces and (b) a region exhibiting a higher degree of roughness. The arrows in panel (a) indicate molecular steps. Reprinted from [11], © 1997, with permission from Elsevier Science.

corrugation is higher, we did not find smooth flat terraces.

STM-excited EL spectra collected on smooth and rough regions show clear differences (Figure 10): The film regions characterized by smoother surfaces exhibit spectra with a distinct and narrow dominant peak at $h\nu = 1.8 \pm 0.03$ eV and a weaker peak at $h\nu = 1.98 \pm 0.03$ eV, both having a linewidth of ~100 meV (FWHM), whereas on the regions with rougher surface morphology, the intensity of the second peak is much higher [10]. Actually, the spectra appear to arise from a linear superposition of spectra from two different kinds of Alq,, e.g., polymorphic forms or shape isomers. As discussed in Section 3, this is also a possible explanation for the double distribution of injection thresholds found in the z–V curves of this material. We note that the spectra are red-shifted with respect to the emission from Alq, in OLED devices, which normally peaks at about 2.3 eV (compare for example [38]). This shift appears to be induced by the intrinsic fluorescence of the tip-Au(111) tunneling junction [10], which arises from the enhanced radiative decay of collective excitations, i.e., plasmons, involving the tip and the metallic surface [50]. This shows that collective excitations (plasmons) involving the tip and the substrate can play an important role in the excitation of light emission, particularly for very thin organic films. Measurements show that the luminescence efficiency increases with the organic thin-film thickness, which suggests quenching of the Alq, emission due to the proximity of the metal surface.

Figure 11 shows a curve representing STL intensity $I_{\rm L}$ vs. $V_{\rm T}$, collected on an Alq₃ thin film deposited on Au(111). The curve is the average of several I_1 –V curves collected on different spots of the sample. Owing to statistical noise, the error in the EL threshold determination is somewhat higher than that for the injection threshold determined from z–V curves. Nevertheless, the energy difference between the EL thresholds of light emission for each of the charge carriers agrees reasonably well with the z–V spectroscopy results; see Section 3. Typically we find that the slope of the I_1 vs. $V_{\rm T}$ curves for positive tip polarity is approximately twice as high as for negative tip polarity. This higher EL efficiency for positive tip polarity is an indication of a different charge-carrier balance for different tip polarities: For positive tip polarity, hole (minority charge carrier) injection into the organic material is more efficient than for negative tip polarity; i.e., the ratio of the hole and electron currents, $i_{\rm b}/i_{\rm e}$, is higher for positive tips, thus giving rise to an increase of radiative recombination events within the organic material.

Finally, it is interesting to consider STL as a technique for degradation studies of organic materials. Regarding the tip/organic material/substrate system as a model

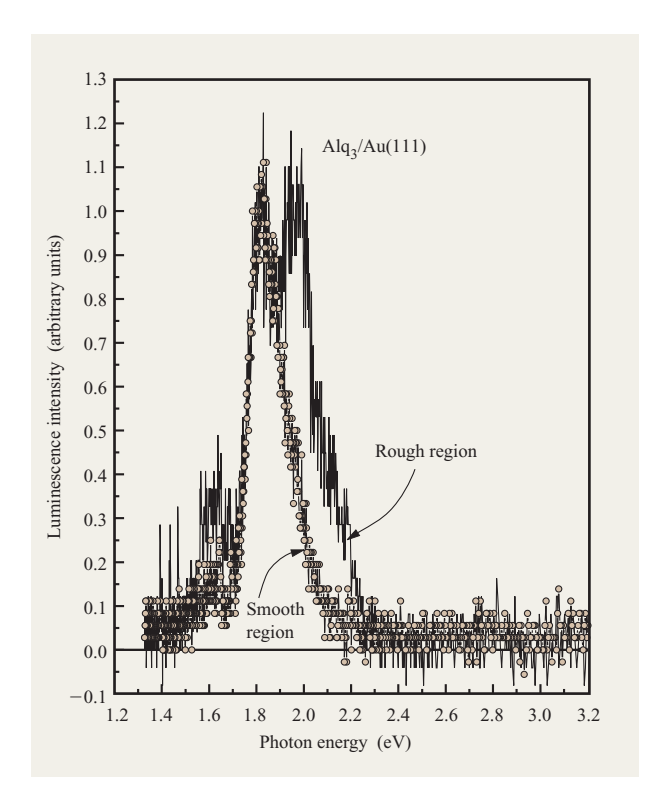


Figure 10

STM-excited electroluminescence spectra collected on a flat terrace and a region of high corrugation of the sample in Figure 9(a) and (b), respectively, at a tip bias of -4.5 V and a tunneling current of 200 pA.

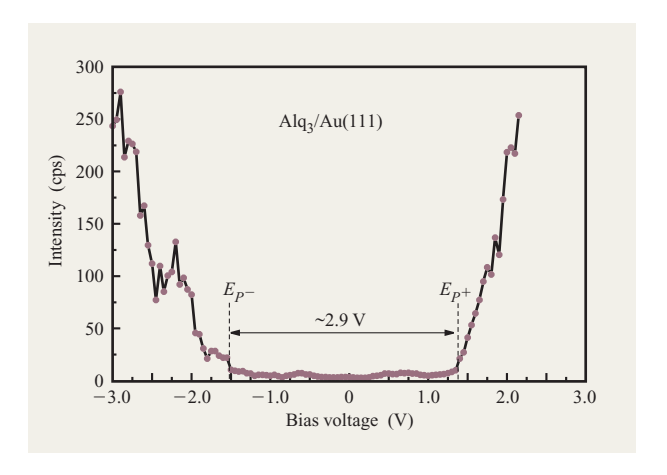


Figure 11

Curve showing typical wavelength-integrated STL intensity $I_{\rm L}$ vs. $V_{\rm T}$, collected at a tunneling current of $i_{\rm T}=150$ pA on an Alq₃ thin film deposited on Au(111).

OLED, our typical experimental parameters correspond to current densities in the range of 10 to 10⁴ A/cm² for bias

voltages well below 10 V. Such enormous current densities are attainable because of the extremely high fields at the apex of the STM tip. Thus, the STM can be used to perform accelerated aging experiments at current density levels not attainable in a standard planar OLED. Conventional OLEDs often show a decrease in the EL intensity, which depends on the amount of charge having passed through the device. In one study [51], the dependence of the time to half brightness was found to have the form $\tau_{1/2} \propto j^{-x}$, where $1.5 \leq x \leq 1.8$. From this expression we can extrapolate to obtain the half time of an OLED operated at the typical device current densities of 1–10 mA/cm². For example, from measurements performed under ultrahigh-vacuum conditions on the conjugated polymer PPV operating at an estimated current density of $j \approx 2 \text{ kA/cm}^2$ and a voltage of $V_T \approx 4.6 \text{ V}$, the time to half brightness is several hours [11]. From the above expression we extrapolate that for an OLED device operated at 10 mA/cm², the half lifetime would exceed tens of thousands of hours even for the typically claimed Coulomb aging case in which x = 1. Preliminary results for Alq, show similar decay behavior, indicating that some organic materials are sufficiently stable so as not to be the limiting factor in obtaining the lifetimes of tens of thousands of hours required for device applications, e.g., for emissive displays.

7. Concluding remarks

STM-based tip-contact techniques have been presented that allow the local electronic and transport properties of organic materials to be probed. STM imaging is used primarily to select and define the location of an experiment. It is then possible to probe a) the barrier heights for injection of positive and negative charge carriers across interfaces; b) the energy gap for single charge-carrier injection; c) the exciton binding energy; and d) charge-carrier transport properties such as the qualitative differences between electron and hole mobilities. In addition, STM-excited luminescence (STL) measurements have been used to study the local electronic excitations of thin organic layers. In the case of Alq₃, for example, we find that the spectral features of the luminescence depend on the structural details of the film, possibly indicating the effects of different polymorphic and/or isomeric forms.

The STL and z–V spectroscopy techniques complement and far exceed the capabilities of photoelectron emission spectroscopy (PES), the standard technique used to study the energy-level alignment at interfaces, which can probe only the HOMO levels and has limited spatial resolution.

Acknowledgments

Many thanks to R. R. Schlittler for technical assistance, T. Beierlein for growing the NPB layers, R. Beyeler for help characterizing the thin-film samples, E. Delamarche and A. Bietsch for preparing gold and silver substrates, and W. Andreoni, A. Curioni, M. Kemerink, and H. W. M. Salemink for many interesting and enlightening discussions. Thanks also to H. Riel for providing the optical absorption measurements on Alq₃, NPB, and CuPc thin films.

References and note

- W. Schottky, Z. Phys. 118, 539 (1942); see also W. Mönch, Surf. Sci. 132, 92 (1983).
- K. Sugiyama, D. Yoshimura, T. Miyamae, T. Miyazaki, H. Ishii, Y. Ouchi, and K. Seki, J. Appl. Phys. 83, 4928 (1998); H. Ishii and K. Seki, IEEE Trans. Electron Devices 44, 1295 (1997); K. Seki, E. Ito, and I. Ishii, Synth. Met. 91, 137 (1997).
- A. Rajagopal, C. I. Wu, and A. Kahn, J. Appl. Phys. 83, 2649 (1998); I. G. Hill, A. Rajagopal, A. Kahn, and Y. Hu, Appl. Phys. Lett. 73, 662 (1998).
- S. T. Lee, X. Y. Hou, M. G. Mason, and C. W. Tang, Appl. Phys. Lett. 72, 1593 (1998).
- T. Mori, H. Fujikawa, S. Tokito, and Y. Taga, *Appl. Phys. Lett.* 73, 2763 (1998).
- R. Schlaf, B. A. Parkinson, P. A. Lee, K. W. Nebesny, and A. R. Armstrong, J. Phys. Chem. B 103, 2984 (1999).
- S. C. Veenstra, U. Stalmach, V. V. Krasnikov,
 G. Hadziioannou, H. T. Jonkman, A. Heres, and
 G. Sawatsky, Appl. Phys. Lett. 76, 2253 (2000).
- 8. I. H. Campbell, T. W. Hagler, D. L. Smith, and J. P. Ferraris, *Phys. Rev. Lett.* **76**, 1900 (1996).
- G. L. J. A. Rikken, Y. A. R. R. Kessener, D. Braun, E. G. J. Staring, and A. Demandt, *Synth. Met.* 67, 115 (1994).
- S. F. Álvarado, L. Libioulle, and P. F. Seidler, *Synth. Met.* 91, 69 (1997).
- S. F. Alvarado, W. Riess, and P. F. Seidler, *Phys. Rev. B* 56, 1269 (1997).
- (a) S. F. Alvarado, P. F. Seidler, D. G. Lidzey, and D. D. C. Bradley, *Phys. Rev. Lett.* 81, 1082 (1998); (b)
 L. Rossi, S. F. Alvarado, W. Riess, S. Schrader, D. G. Lidzey, and D. D. C. Bradley, *Synth. Met.* 111–112, 527 (2000).
- R. N. Marks, J. J. M. Halls, D. D. C. Bradley, R. H. Friend, and A. B. Holmes, *J. Phys. Cond. Mater.* 6, 1379 (1994).
- S. Barth, S. Deussen, and H. Bässler, *Phil. Trans. Roy. Soc. Lond. A* 355, 749 (1997); S. Barth and H. Bässler, *Phys. Rev. Lett.* 79, 4445 (1997).
- E. L. Frankevich, A. A. Lymarev, I. Sokolik, F. F. Karacz,
 S. Blumenstengel, R. H. Baughman, and H. H. Hörhold,
 Phys. Rev. B 46, 9320 (1992).
- M. Scheidler, U. Lemmer, R. Kerstin, S. Karg, W. Riess, B. Cleve, R. F. Mart, H. Kurz, H. Bässler, E. O. Göbel, and P. Thomas, *Phys. Rev. B* 54, 5536 (1996).
- C. H. Lee, G. Yu, D. Moses, and A. J. Heeger, *Phys. Rev.* B 49, 2396 (1994).
- J. M. Leng, S. Jeglinski, X. Wei, R. E. Benner, Z. Vardeny, F. Guo, and S. Mazumdar, *Phys. Rev. Lett.* 72, 156 (1994)
- M. Chandross, S. Mazumdar, S. Jeglinski, X. Wei, Z. V. Vardeny, E. W. Kwock, and T. M. Miller, *Phys. Rev. B* 50, 14702 (1994).
- S. A. Van Slyke, C. H. Chen, and C. W. Tang, *Appl. Phys. Lett.* 69, 2160 (1996).

- S. A. Van Slyke and C. W. Tang, U.S. Patent 4,720,432, 1988; C. Adachi, K. Nagai, and N. Tamoto, *Appl. Phys. Lett.* 66, 2679 (1995).
- C. W. Tang and S. A. Van Slyke, *Appl. Phys. Lett.* 51, 913 (1987); C. W. Tang, S. A. Van Slyke, and C. H. Chen, *J. Appl. Phys.* 65, 3610 (1989).
- 23. See for example R. Feenstra, Phys. Rev. B 50, 4561 (1994); C. Julian Chen, Introduction to Scanning Tunneling Microscopy, Oxford Series in Optical and Imaging Sciences, M. Lapp, J.-I. Nishizawa, B. B. Snavely, H. Stark, A. C. Tam, and T. Wilson, Eds., Oxford University Press, New York, 1993; R. Wiesendanger, Scanning Probe Microscopy and Spectroscopy, Methods and Applications, Cambridge University Press, Cambridge, England, 1994.
- E. M. Conwell and E. W. Wu, Appl. Phys. Lett. 70, 1867 (1997).
- M. N. Bussac, D. Michoud, and L. Zuppiroli, *Phys. Rev. Lett.* 81, 1678 (1998).
- M. A. Lampert and P. Mark, Current Injection in Solids, H. G. Booker and N. DeClaris, Eds., Academic Press, Inc., New York, 1970.
- See for instance A. van der Ziel, in Solid State Physical Electronics, W. L. Everitt, Ed., Prentice-Hall, Inc., Englewood Cliffs, NJ, 1968.
- 28. The phenomenon of tip penetration as a function of tunneling voltage has been reported previously for organic materials. To our knowledge, however, no attempt has been made to determine electronic levels from those measurements; see for instance F. G. C. Hogenraad, A. C. R. Hogervorst, P. M. L. O. Scholte, and F. Tunistra, *Ultramicrosc.* 42–44, 1004 (1992); W. Mizutani, M. Shigeno, Y. Sakakibara, K. Kajimura, M. Ono, S. Tanishima, K. Ohno, and N. Toshima, *J. Vac. Sci. Technol. A* 8, 675 (1990).
- M. Brinkmann, G. Gadret, M. Muccini, C. Taliani, N. Masciocchi, and A. Sironi, J. Amer. Chem. Soc. 122, 5147 (2000).
- 30. H. B. Michaelson, J. Appl. Phys. 48, 4729 (1977).
- 31. C. Hosokawa, H. Higashi, H. Nakamura, and T. Kusumoto, *Appl. Phys. Lett.* **67**, 3853 (1995).
- 32. M. Matsumura and T. Akai, *Jpn. J. Appl. Phys.* **35**, 5357 (1996).
- 33. M. Probst and R. Haight, Appl. Phys. Lett. 71, 202 (1997).
- A. Schmidt, M. L. Anderson, and N. R. Armstrong, J. Appl. Phys. 78, 5619 (1995).
- S. T. Lee, Y. M. Wang, X. Y. Hou, and C. W. Tang, Appl. Phys. Lett. 74, 670 (1999).
- 36. E. M. Conwell, Synth. Met. 83, 101 (1996).
- A. Curioni, M. Boero, and W. Andreoni, *Chem. Phys. Lett.* 294, 263 (1998).
- P. E. Burrows, Z. Shen, V. Buloic, D. M. McCarty, S. Forrest, J. A. Cronin, and M. E. Thompson, J. Appl. Phys. 79, 7991 (1996).
- H. Riel, Diplomarbeit, Institut für Technische Physik I, Friedrich-Alexander Universität, Erlangen-Nürenburg, Germany, April 1998.
- L. Rossi, P. Müller, S. F. Alvarado, and W. Riess, Proceedings of E-MRS, Strasbourg, France, May 30– June 2, 2000 (to be published in Synthetic Metals).
- G. Parthasarathy, P. E. Burrouws, V. Kalfin, V. G. Kozlov, and S. R. Forrest, *Appl. Phys. Lett.* 72, 2138 (1998)
- 42. P. M. Borsenberger and D. S. Weiss, *Organic Photo Receptors for Imaging Systems*, Marcel Dekker, Inc., New York, 1993, and references therein.
- R. G. Kepler, P. M. Beeson, S. J. Jacobs, R. A. Anderson, M. B. Sinclair, V. S. Valencia, and P. A. Cahill, *Appl. Phys. Lett.* 66, 3618 (1995); T. Tsutsui, H. Tokuhisa, and M. Era, *Proc. SPIE* 3281, 230 (1998).
- 44. A. G. Mückl, S. Berleb, W. Brütting, and M. Schwoerer, *Synth. Met.* **111–112**, 91 (2000).

- I. I. Smolyaninov and M. S. Khaikin, *Phys. Lett. A* 149, 410 (1990);
 I. I. Smolyaninov, *Surf. Sci.* 364, 135 (1996).
- 46. E. Flaxer, O. Sneh, and O. Chesnovski, *Science* **262**, 2012 (1993).
- D. G. Lidzey, S. F. Alvarado, P. F. Seidler, A. Bleyer, and D. D. C. Bradley, *Appl. Phys. Lett.* 71, 2008 (1997).
- 48. D. G. Lidzey, D. D. C. Bradley, S. F. Alvarado, and P. F. Seidler, *Nature* **386**, 135 (1997).
- J. V. Barth, H. Burne, G. Ertl, and R. J. Behm, *Phys. Rev.* B 42, 9307 (1990).
- 50. R. Berndt and J. K. Gimzewski, *Phys. Rev. Lett.* **67**, 3796 (1991), and references therein.
- Y. Sato, S. Ichinosawa, and H. Kanai, in *Inorganic and Organic Electroluminescence*, R. H. Mauch and H.-L. Gummlich, Eds., Wissenschaft und Technik, Berlin, 1996, p. 225.

Received June 30, 2000; accepted for publication September 13, 2000

Santos F. Alvarado IBM Research, Zurich Research Laboratory, 8803 Rüschlikon, Switzerland (alv@zurich.ibm.com). In 1974 Dr. Alvarado received an undergraduate degree in physics at the Instituto de Física y Matemáticas, Instituto Politécnico Nacional de México, in Mexico City, Mexico, and in 1977 a Ph.D. degree in physics from the Eidgenössische Technische Hochschule in Zurich, Switzerland. His thesis pertained to the topic of spin-polarized photoelectron spectroscopy on magnetic transition-metal oxides. In 1978, as a Postdoctoral Fellow, he was affiliated with the Kernforschungsanlage Jülich (KFA), in Jülich, Germany, where a few years later he became a Research Staff Member. At the KFA he initiated a project on spin-polarized, lowenergy electron diffraction for the study of surface magnetism. The project also included the preparation of optically pumped spin-polarized electron sources from molecular-beam epitaxygrown III-V thin films and heterostructures. In 1986, he joined the IBM Zurich Research Laboratory, where he initiated a project on scanning tunneling microscopy (STM) of magnetic materials with spin-polarized electron detection by light emission. Dr. Alvarado's present research interests involve the study of the electronic properties of organic materials for light-emitting device applications.

Laura Rossi FIDEURAM Capital S.p.A., Via S. Paolo, 10, 20121 Milano, Italy (lrossi@fideuramcapital.it). Dr. Rossi received a degree in physics from the University of Pavia, Italy, in 1993. For her thesis on the photophysics of organic materials useful for application in light-emitting devices (LEDs), in particular small molecules and conjugated polymers, she received a Ph.D. degree in 1997. During her two-year stay at the IBM Zurich Research Laboratory in Switzerland as a Postdoctoral Fellow, she worked on the application of novel STM-based spectroscopic techniques to the study of intrinsic transport properties of organic materials that are basic constituents of a multilayer LED structure. Dr. Rossi has since moved into the field of finance and is now at Fideuram Capital S.p.A. in Milan, Italy. Her new field of research is the development of assets and liability management models using multistage stochastic programming.

Peter Müller IBM Research, Zurich Research Laboratory, 8803 Rüschlikon, Switzerland (pmu@zurich.ibm.com). Mr. Müller is a Research Staff Member at the IBM Zurich Research Laboratory. He is currently involved in the OLED project, where his main interests are electrified interfaces. He joined IBM in 1987 after having received a degree in computer science from the Brugg-Windisch Polytechnical Institute in Switzerland. From 1994 to 1996, he was a Guest Scientist at the Exploratory Research and Technology Organization (ERATO) at Tohoku University, Japan.

Paul F. Seidler IBM Research, Zurich Research Laboratory, 8803 Rüschlikon, Switzerland (pfs@zurich.ibm.com). Dr. Seidler is Manager of Science and Technology at the IBM Zurich Research Laboratory. His department pursues research in the fields of micromechanics, molecular-scale engineering, display technology, optical communications, advanced materials processing and characterization, and computational materials science. Dr. Seidler received a B.S. degree in chemistry from the California Institute of Technology in 1980 and a Ph.D. degree in chemistry from the University of California at Berkeley in 1985 for his thesis in the field of mechanistic organometallic chemistry. After a postdoctoral fellowship at Exxon Corporate Research, he joined the IBM

Thomas J. Watson Research Center, where he worked on a variety of scientific studies related to semiconductor processing technology, in particular the kinetics and mechanisms of metal chemical vapor deposition. After serving a year as Technical Assistant to the Vice President, Systems, Technology and Science for the IBM Research Division, he moved to the Zurich Research Laboratory to become head of the Display Technology group and the IBM organic lightemitting diode project.

Walter Riess IBM Research, Zurich Research Laboratory, 8803 Rüschlikon, Switzerland (wri@zurich.ibm.com). Dr. Riess received a degree in physics (Dipl. Phys.) from the University of Bayreuth, Germany, in 1987. In 1991, he received a Ph.D. degree from the University of Bayreuth for his thesis on nonlinear conduction phenomena in organic charge density wave conductors. From 1992 to 1995, he was a research assistant in the Physical Institute of the University of Bayreuth, where he investigated charge-carrier injection, transport, and recombination processes in organic lightemitting diodes. During his stay as a visiting scientist at the IBM Zurich Research Laboratory in 1994, Dr. Riess initiated a project on organic light-emitting diodes; in October 1995, he joined the IBM Zurich Research Laboratory as a Research Staff Member in the Display Technology group. Dr. Riess finished his habilitation in 1996 with a thesis on polymeric light-emitting diodes. In October 1998, he became manager of the Display Technology group and continues to focus on display applications of electroluminescent organic materials.

100